Redox Biology 62 (2023) 102670

Contents lists available at ScienceDirect

Redox Biology

journal homepage: www.elsevier.com/locate/redox

Hydrogen peroxide production by epidermal dual oxidase 1 regulates nociceptive sensory signals

Anna Pató [a], Kata Bölcskei [b], Ágnes Donkó [a], Diána Kaszás [a,c,d], Melinda Boros [b], Lilla Bodrogi [g], György Várady [h], Veronika F.S. Pape [a], Benoit T. Roux [a,c,d], Balázs Enyedi [a,c,d], Zsuzsanna Helyes [b,e,f], Fiona M. Watt [i], Gábor Sirokmány [a,1,**], Miklós Geiszt [a,1,*]

[a] Department of Physiology, Semmelweis University, Faculty of Medicine, H-1094, Budapest, Hungary
[b] Department of Pharmacology and Pharmacotherapy, Medical School, University of Pécs, H-7624, Pécs, Hungary
[c] MTA-SE Lendület Tissue Damage Research Group, Hungarian Academy of Sciences and Semmelweis University, H-1094, Budapest, Hungary
[d] HCEMM-SE Inflammatory Signaling Research Group, Department of Physiology, Semmelweis University, H-1094, Budapest, Hungary
[e] Eötvös Lorand Research Network, Chronic Pain Research Group, University of Pécs, H-7624, Pécs, Hungary
[f] National Laboratory for Drug Research and Development, Magyar tudósok krt. 2, H-1117, Budapest, Hungary
[g] Department of Animal Biotechnology, Institute of Genetics and Biotechnology, Hungarian University of Agriculture and Life Sciences, H-2100, Gödöllő, Hungary
[h] Research Centre for Natural Sciences, Institute of Enzymology, H-1117, Budapest, Hungary
[i] European Molecular Biology Laboratory, 69117, Heidelberg, Germany

ARTICLE INFO

Keywords:
NADPH oxidase
Hydrogen peroxide
Dual oxidase 1
DUOX1
Skin
Nociception

ABSTRACT

Keratinocytes of the mammalian skin provide not only mechanical protection for the tissues, but also transmit mechanical, chemical, and thermal stimuli from the external environment to the sensory nerve terminals. Sensory nerve fibers penetrate the epidermal basement membrane and function in the tight intercellular space among keratinocytes. Here we show that epidermal keratinocytes produce hydrogen peroxide upon the activation of the NADPH oxidase dual oxidase 1 (DUOX1). This enzyme can be activated by increasing cytosolic calcium levels. Using DUOX1 knockout animals as a model system we found an increased sensitivity towards certain noxious stimuli in DUOX1-deficient animals, which is not due to structural changes in the skin as evidenced by detailed immunohistochemical and electron-microscopic analysis of epidermal tissue. We show that DUOX1 is expressed in keratinocytes but not in the neural sensory pathway. The release of hydrogen peroxide by activated DUOX1 alters both the activity of neuronal TRPA1 and redox-sensitive potassium channels expressed in dorsal root ganglia primary sensory neurons. We describe hydrogen peroxide, produced by DUOX1 as a paracrine mediator of nociceptive signal transmission.

Our results indicate that a novel, hitherto unknown redox mechanism modulates noxious sensory signals.

1. Introduction

Epidermal keratinocytes serve not only as a mechanical barrier to maintain the homeostatic integrity of our body, but they also function as first responders to a broad range of mechanical, chemical, and thermal inputs from the external environment. They possess several membrane receptors and ion channels that trigger intracellular signaling cascades upon activation by various stimuli. Keratinocytes are also described as the source of several paracrine signaling molecules like prostaglandins, cytokines, nucleotides, and also reactive oxygen species (ROS) [1–4].

Abbreviations: AITC, allyl isothiocyanate; ATPγS, adenosine 5'-(gamma-thiotriphosphate); BIAM, biotin polyethyleneoxide iodoacetamide; DMSO, dimethyl sulfoxide; DPA, dynamic plantar aesthesiometer; DRG, dorsal root ganglion; DUOX1, dual oxidase 1; HEK, human embryonic kidney; HRP, horse radish peroxidase; KCNQ4, potassium voltage-gated channel subfamily Q member 4; KO, knock out; PBS, phosphate buffered saline; PCR, polymerase chain reaction; PEG_2, prostaglandin E_2; PMSF, phenylmethylsulfonyl fluoride; ROS, reactive oxygen species; siRNA, short interfering ribonucleic acid; TRPA1, transient receptor potential ankyrin 1; TRPV4, transient receptor potential vanilloid 4; WT, wild type.

* Corresponding author.
** Corresponding author.
E-mail addresses: sirokmany.gabor@med.semmelweis-univ.hu (G. Sirokmány), geiszt.miklos@med.semmelweis-univ.hu (M. Geiszt).
[1] These authors contributed equally to this work.

https://doi.org/10.1016/j.redox.2023.102670
Received 22 January 2023; Received in revised form 22 February 2023; Accepted 13 March 2023
Available online 15 March 2023

These secreted substances can mediate intercellular communication in the skin.

The detailed histological analysis of mammalian skin in previous studies revealed the presence of unmyelinated nerve fibers in the epidermis [5,6]. These polymodal sensory nerve fibers penetrate the dermal-epidermal basement membrane and interweave among the very tightly organized epidermal cell layers. Epidermal nerve fiber density (ENFD) is a clinically important histological marker in several neuropathic conditions [7]. The close proximity of nerve fibers and keratinocytes renders the latter suitable to function as a secondary sensory cell that can trigger or modulate the activation of the sensory neuron. The narrow, almost virtual intercellular space between epidermal keratinocytes might contribute to high local concentrations of paracrine mediators around the activated epithelial cells.

Both acute inflammatory and persistent inflammatory and neuropathic pain have previously been reported to be enhanced by the presence of ROS [8–10]. Although various leukocyte and neuronal sources of ROS production have been identified that mediate these pro-algesic effects of ROS, relatively little is known about the role of ROS produced by keratinocytes. The biological effects of ROS released locally, frequently, and repeatedly by keratinocytes may significantly differ from the effects of ROS from white blood cells and nerve fibers during invasive tissue injury.

ROS can be formed as a byproduct of several metabolic pathways but there is also a group of enzymes – the NADPH oxidase family - devoted specifically to the regulated production of ROS. Members of the NADPH oxidase family typically do not have a ubiquitous, widespread distribution but rather show a specific, unique expression pattern. According to previous reports and publicly available expression databases DUOX1 is expressed in the mammalian skin [4,11]. Our goal was to characterize the expression and activity of DUOX1 in the mammalian skin in more detail and reveal its potential biological functions.

Here we show that several different signaling pathways that lead to intracellular calcium signals in keratinocytes can induce the release of H_2O_2. We provide evidence that the major source of this calcium-dependent peroxide production of keratinocytes is the NADPH oxidase family member dual oxidase 1 (DUOX1).

We analyzed the noxious behaviors of wild-type and DUOX1 deficient animals following the application of cutaneous nociceptive stimuli and we found increased thermal hyperalgesia in DUOX1 knockout mice.

Our results indicate that DUOX1-derived H_2O_2 induces redox-dependent changes in the Kcnq4 (Kv7.4) voltage-gated potassium channel and may also modulate the Transient Receptor Potential Ankyrin Repeat 1 (TRPA1) non-selective cation channel activity.

Based on our *in vivo* and *in vitro* results we propose a new model where the DUOX1-dependent peroxide production of keratinocytes triggers redox changes in cell membrane potassium channel and TRPA1 channel activity in peripheral nerve fibers of dorsal root ganglia. Thereby keratinocyte-derived H_2O_2 can alleviate the sensitivity and responsiveness of sensory nerve fibers in a paracrine fashion.

2. Methods

2.1. Cell culture

HEK293 (ATCC, Manassas, VA, USA, CRL-1573), HEK293T (ATCC, Manassas, VA, USA, CRL-3216), HEK293A (Invitrogen R705-07) and HaCaT cells (ATCC, Manassas, VA, USA) were cultured in Dulbecco's Modified Eagle's Medium (DMEM; Lonza Group Ltd., Basel, Switzerland) supplemented with 100 U/ml penicillin, 100 U/ml streptomycin (Lonza Group Ltd., Basel, Switzerland) and 10% fetal bovine serum (FBS; Lonza Group Ltd., Basel, Switzerland). Cells were grown in a humidified incubator with 5% CO_2 in air, at 37 °C.

Primary mouse keratinocytes were prepared from the back skin of wild-type and Duox1 deficient mice as described previously [12].

2.2. Animals

DUOX1 knockout mice described earlier by Donkó et al. [13] were purchased from Lexicon Pharmaceuticals, Inc. (The Woodlands, TX, USA). C57BL/6N wild-type mice were obtained from commercial sources. Experimental animals were maintained on a standard diet and given water *ad libitum* in either specific pathogen-free or conventional animal facilities of Basic Medical Science Centre, Semmelweis University.

Animals for nociception assays were kept in the animal house of Szentágothai Research Centre, University of Pécs, in individually-ventilated cages on wood shavings bedding, at 22 ± 2 °C temperature and a standard 12-12 h light-dark cycle (lights on between 7:00–19:00). They were provided with standard rodent chow and water *ad libitum*. All experiments were designed and performed according to the 243/1998. Hungarian government regulation on animal experiments. Experiments were approved by the Ethics Committee on Animal Research of the University of Pécs (license number: BA02/2000-10/2011).

10–12 week old male mice of each genotype were used up to the necessary sample size. Sample size was determined based on our previous experiments using the same models [14] considering also the 3R (replace, reduce, refine) rule for the animal ethical principles. The animals were randomized in the different experimental groups, the researchers were blinded to the experimental design, the treatment the animals received, and the genotype. Due to short-term anaesthesia and short observation times, the general health status of animals was not affected. The analysis included the results of all tested animals, there were no exclusions.

2.3. Mustard oil-induced thermal hyperalgesia on the tail

The noxious heat threshold of the tail of mice was measured with an increasing-temperature water bath (Experimetria Ltd., Budapest, Hungary) as previously described [14]. Mice were placed into plastic restrainers which were hanged on a rack above the water bath so that the tails could be immersed into the water. The following parameters were set on the device: a starting temperature of 30 °C, a heating rate of 24 °C/min and a cut-off temperature of 53 °C. The heating was immediately stopped when the animals showed nocifensive behavior and the tails were removed from the water. The corresponding water temperature was recorded as the noxious heat threshold. After 3 control treshold measurements, thermal hyperalgesia was induced by immersing the tails into 5% mustard oil dissolved in 30% DMSO in water for 30 s. Noxious heat threshold measurements were repeated at 10 min intervals for 60 min after treatment. Where indicated, 3 mg/kg intraperitoneal naloxone pretreatment had been applied.

2.4. Heat injury-induced thermal and mechanical hyperalgesia on the paw

The noxious heat threshold of the paws of freely-moving mice was measured with an increasing-temperature hot plate (IITC Life Sciences, Woodland Hills, CA, USA), while the mechanonociceptive threshold was determined by a dynamic plantar aesthesiometer (DPA; Ugo Basile, Comerio, Italy). The starting temperature on the hot plate was set to 30 °C and a heating rate of 12 °C/min and cut-off temperature of 53 °C were used. For the mechanical stimulation, the DPA device uses a blunt needle pushed at the plantar surface of the paw at an increasing force, which was set to 2 g/s up to a cut-off value of 10 g. For both methods, stimulation was immediately stopped when the animal showed nocifensive behavior and the corresponding temperature or force was recorded as the threshold. After 3 control threshold measurements, heat injury (i.e. a first-degree burn model) was induced under ether anaesthesia by immersing one of the hind paws into 51 °C water for 15 s. Noxious thermal or mechanical thresholds were measured for 60 min at 10 min intervals afterwards [15].

2.5. Plantar incision-induced mechanical hyperalgesia on the paw

Mechanical thresholds were measured by the DPA, as described above. A postoperative pain model was induced by making a 5-mm incision on the paw, under ketamine-xylazine anaesthesia (100-5 mg/kg i.p.). The incision was closed with 4/0 silk sutures and animals were allowed to recover for 24 h. Thresholds were measured afterwards once per day for 3 days after surgery [16].

2.6. Formalin test

For the evaluation of formalin-induced nociception, mice were injected intraplantar with 2.5% formalin (20 μl, i.pl.) and then placed into transparent observation chambers. A mirror was placed behind the chamber so that the observer could see the animals from behind. Spontaneous nocifensive behavior was assessed between 0-5 min and 20–45 min after injection, based on the characteristic 2-phase response induced by formalin. The duration of paw licking was measured by a stopwatch, while paw flinching responses were counted. A Composite Pain Score (CPS) was also calculated by the following formula: CPS=(2x paw licking time + 1x paw flinchings)/observation time. The swelling induced by formalin was determined 3 h after injection by measuring the thickness of the paw with a digital caliper (Mitutoyo, Kawasaki, Japan). The swelling was expressed as a % increase compared to the contralateral paw.

2.7. Histology and immunostaining

Tissues were fixed in formal saline and embedded in paraffin blocks. For routine histology and immunostaining, 5 μm thick sections were cut. These were either stained with haematoxylin and eosin or went through heat induced epitope retrieval (HIER) in citrate buffer (10 mM sodium citrate, pH 6.0) before overnight incubation with specific first antibodies. To be able to detect PGP9.5-positive nerve fibers in the epidermis, 100 μm thick paraffin sections were cut. These were also processed through HIER and the floating thick skin sections were incubated overnight with rabbit polyclonal anti-PGP9.5 antibodies. Multiple Z-stack images acquired on a Leica SP5 laser scanning microscope, using a 20x HCX PL APO CS dry objective were merged to obtain the final images. For Tuj-1 wholemount labeling tail skin was slit lengthways with a scalpel, peeled off and cut into 5 × 5 mm pieces, and incubated in 5 mM EDTA in PBS at 37 °C for 4 h. The intact sheet of epidermis was gently peeled away from the dermis and the epidermal tissue was fixed in 4% formal saline for 2 h at room temperature [17]. Fixed epidermal sheets were blocked, permeabilized and incubated overnight with Tuj-1 antibody. After extensive washing steps (6 × 30 min), the secondary fluorescent antibody was added for 4 h, and after further washing steps, the epidermal tissue pieces were mounted on glass slides.

Primary antibodies: keratin-10, keratin-14, loricrin and gamma-catenin antibodies were from Covance Research Products, Inc. (now BioLegend). Connexin-43 antibody (#3512) was from Cell Signaling Technology, Danvers, Massachusetts, USA, Tuj-1 antibody (sc-58888) was from Santa Cruz Biotechnology Inc, Dallas, Texas, USA. PGP9.5 antibody (ab8189) was from Abcam, Cambridge, UK. Alexa488 or Alexa568 coupled secondary antibodies were from ThermoFisher Scientific.

2.8. Electron microscopy

Sample preparation and imaging were carried out as described previously [18,19]. Briefly, adult mice were anesthetized with ketamine (0.4 ml/100g, 0.2 ml/mouse i.p.), then were transcardially perfused with 0.9% saline for 1 min followed by the fixative: 4% paraformaldehyde, 15% picric acid, 0.05% glutaraldehyde made up in 0.1 M phosphate buffer for 30 min. Sections for electron microscopy were postfixed with 0.5–1% OsO_4, contrasted in 1% uranyl acetate, dehydrated in graded alcohol series, and embedded into epoxy resin. Sections were examined with a transmission electron microscope (TEM, JEM1011, Jeol).

2.9. Quantitative PCR

Mouse tissue RNA was isolated from dorsal root ganglions (DRG), hindpaw and tail skin using RNeasy Mini Kit (Qiagen, Hilden, Germany). Human keratinocyte RNA was purified using NucleoSpin RNA (Macherey-Nagel, Düren, Germany). Before the RNA preparation, tissue sample were collected into RNAlater reagent (Thermo Fisher Scientific, Waltham, MA, USA) at room temperature. The concentration of the RNA samples was tested by ultraviolet absorption at 260/280 nm in Nano Drop One system (Thermo Fisher Scientific, Waltham, MA, USA). cDNA was synthesized from 2 μg of total RNA using High-Capacity cDNA Reverse Transcription Kit (Fermentas) according to the manufacturer's recommendations. For qPCR reaction 0.5 μl of cDNA was used in a 10 μl reaction solution using Taqman Gene Expression Assays (Thermo Fisher Scientific, Waltham, MA, USA) and LightCycler 480 Probes Master (Roche Life Science) in a LightCycler LC480 plate reader (Roche Life Science). For each cDNA sample, the expression of the target was divided by the expression of the endogenous control, which was eukaryotic elongation factor 2 (Eef-2) or GAPDH. The crossing point was determined by the second derivative method.

The following Taqman Gene Expression assays were used.

2.9.1. Mouse

Nox1: Mm00549170_m1, Cybb: Mm01287743_m1, *Nox4*: Mm00479246_m1, *Duox1*: Mm01328698_m1, *Duox2*: Mm01326247_m1, *DuoxA1*: Mm01269313_g1, *DuoxA2*: Mm00470560_m1, *Eef-2*: Mm01171434_g1, *Kcnq4*: Mm01185500_m1, *TrpA1*: Mm01227437_m1, *TrpV1*: Mm01246302_m1, *TrpV3*: Mm00455003_m1, *TrpV4*: Mm00455003_m1, *Dpp6*: Mm00456620_m1, *DPP10*: Mm01284949_m1, *Kcnd3*: Mm01302126_m1, *Kcnd1*: Mm00492793_g1, *Gapdh*: Mm99999915_g1.

2.9.2. Human

NOX1: Hs00246589_m1, *CYBB*: Hs00166163_m1, *NOX3*: Hs01098883_m1, *NOX4*: Hs00418356_m1, *NOX5*: Hs00225846_m1, *DUOX1*: Hs00213694_m1, *DUOX2*: Hs00204187_m1, *DUOXA1*: Hs00328806_m1, *DUOXA2*: Hs01595311_g1, *CYBA*: Hs03044361_m1, NOXO1: Hs00376045_g1, NOXA1: Hs00736699_m1, *GAPDH*: Hs99999905_m1.

2.10. Amplex Red assay

Confluent cells on 24-well plates (SPL Life Sciences Co., Korea) were washed with H-medium (145 mM NaCl, 5 mM KCl, 1 mM $MgCl_2$, 0.8 mM $CaCl_2$, 10 mM HEPES, and 5 mM glucose, pH 7.4) and background fluorescence was also measured in 0.3 ml/well H-medium. For the assay, an H-medium-based reaction solution was used containing horse radish peroxidase (Sigma-Aldrich, Burlington, MA, USA) and Amplex Red (Synchem, Germany) in a final concentration of 0.2 U/ml and 50 μM respectively. Cells were stimulated with 1 μM thapsigargin (Sigma-Aldrich, Burlington, MA, USA) or 10 μM ATPγS (Sigma-Aldrich, Burlington, MA, USA), or 2 nM GSK 1016790A (Sigma-Aldrich, Burlington, MA, USA). Stimuli were also added to the Amplex Red containing reaction solution immediately before pipetting it onto the cells. The measurement of fluorescence started promptly after the addition of the reaction solution and the cells were kept at 37 °C throughout the measurement. Fluorescence of the end-product resorufin was measured at 590 nm with POLARstar Optima multidetection microplate reader (BMG Labtech, Ortenberg, Germany). Background fluorescence was subtracted from the fluorescence values of each well. Each experimental condition was run in 3 parallels on the 24-well plate.

2.11. Measurement of prostaglandin E_2 release

SiRNA-treated HaCaT cells were stimulated with ATPγS and cell culture supernatants were harvested after the indicated incubation times. PGE_2 was measured using the Enzo Life Sciences PGE_2 ELISA kit, according to the manufacturer's instructions. Concentrations were calculated based on a calibration curve.

2.12. Measurement of ATP secretion

HEK293A cells expressing the $GRAB_{ATP}$ sensor were kindly provided by Balázs Enyedi. $GRAB_{ATP}1.0$ expression plasmid was created by Gibson cloning based on the sequence provided in the article of Wu et al. [20]. $GRAB_{ATP}1.0$ was N-terminally fused through a P2A peptide with a plasma membrane localized far-red fluorescent protein, mKate2. Membrane localization of mKate2 was achieved by fusing it to the N-terminal targeting sequence of the protein Lck (MGCVCSSNPENNNN).

35000 cells/well (30% HEK293A-70% HaCaT or 100% HEK293A) were plated on Ibidi 8-well μ-slides (Ibidi GmbH, Gräfelfing, Germany) pretreated with poly-L-lysine (Sigma-Aldrich, Burlington, MA, USA). Next day before measurements, growth medium was replaced with imaging medium (EC1, containing 3.1 mM KCl, 133.2 mM NaCl, 0.5. mM KH_2PO_4, 0.5 mM $MgSO_4$, 5 mM Na-HEPES, 2 mM $NaHCO_3$, 1.2 mM $CaCl_2$ and 2.5 mM Glucose) Experiments were performed at room temperature on a NikonTi2 inverted microscope equipped with an Apo LWD 40x WI λS DIC N2 water immersion objective, a Yokogawa CSU-W1 Spinning Disk unit, a Photometrics Prime BSI camera and 488 nm and 561 nm diode laser lines. After recording the cells for 2 min, a custom-made perfusion system was opened and fresh EC1 medium was delivered by perfusion to wash the previously produced ATP away. As treatment 2.5 nM GSK 1016790A or 500 μM H_2O_2 were applied. At the end of the measurement 1 μM ATP was added as a positive control.

2.13. Analysis and quantification of ATP secretion

$GRAB_{ATP}$ expressing cells were automatically segmented in the red channel (mKate2) using the software Cellpose [21]. The mean intensity of the green and red channel (cpEGFP and mKate2) was recorded for each cell at each time point using the generated masks. Taking advantage of the P2A peptide linker between the mKate2 and $GRAB_{ATP}$ resulting in a 1:1 expression ratio, we used the green/red ratio as a normalized measure of the $GRAB_{ATP}$ signal. To express all intensities between 0 and 1, we applied the following further normalization: $(F–F_0)/(F_{max}-F_0)$, where F is the intensity at a given time point, F_0 is the average intensity value of the baseline measured during the 5 min prior to the stimulation and F_{max} is the maximum intensity value after ATP stimulation. Finally, we applied a rolling average of 3 on the normalized data. The final output data was then denoted $\Delta F/F_0$. For all experiments, we excluded the 2 min pre-prefusion baseline and the first 3 min of the washing step from the analysis.

Prior to analysis, the background intensity was removed automatically using the SMO software (https://doi.org/10.1101/2021.11.09.467975) and images were registered using the pystackreg software (https://doi.org/10.1109/83.650848). All data were analyzed and plotted using the Python libraries.

Pandas https://doi.org/10.25080/MAJORA-92BF1922-00A.

Numpy https://doi.org/10.1038/s41586-020-2649-2.

Seaborn https://doi.org/10.21105/joss.03021.

Statistical analysis was done using the *t*-test of the 'stats' module from the Python library SciPy.

2.14. Calcium imaging

40000 cells/well were plated on 96-well plates (SPL Life Sciences Co., Korea) pretreated with poly-L-lysine (Sigma-Aldrich, Burlington, MA, USA). HEK293 cells were transfected with human TRPA1 expressing plasmid using Lipofectamine 2000 (Invitrogen) according to the manufacturer's instructions. The plasmid was kindly provided by Zoltán Sándor, Department of Pharmacology and Pharmacotherapy, University of Pécs, Medical School [22]. Next day cells were washed with H-medium and loaded with Fura2-AM (2 μM dissolved in H-medium, Molecular Probes, USA) for 30 min at 37 °C. Cells were washed again and the baseline fluorescence was measured using Clariostar (BMG Labtech, Ortenberg, Germany). Excitation wavelengths were 335 and 380 nm, emission wavelength was 510 nm. The final concentrations of different stimuli were as follows: 500 or 100 μM H_2O_2 (Sigma-Aldrich, Burlington, MA, USA) and 10 μM AITC (Sigma-Aldrich, Burlington, MA, USA). Each experimental condition was run in 3 parallels.

2.15. Biotinylation of reduced thiols

HEK293T cells were transfected on poly-L-lysine (Sigma-Aldrich, Burlington, MA, USA) coated 6-well plates (SPL Life Sciences Co., Korea) with Kcnq4 Mouse Tagged ORF Clone (OriGene, Rockville, MD, USA) using Lipofectamine LTX and Plus Reagents (Invitrogen) following the manufacturer's instructions. Next day the transfected cells were washed with H-medium and treated with 0, 20, 100, or 500 μM H_2O_2 in 2 ml H-medium for 3 min at 37 °C. After the treatment cells were lysed and collected in ice-cold lysis buffer (50 mM TRIS, 140 mM NaCl, 1% Triton X-100, 0.1% SDS, 1 mM PMSF, and cOmplete Mini Protease Inhibitor Cocktail (Merck, Darmstadt, Germany), pH 8) with 250 μM biotin polyethyleneoxide iodoacetamide (BIAM, Thermo Fisher Scientific, Waltham, MA, USA). Samples were centrifuged at 15,000 RPM for 10 min at 4 °C and the supernatants were incubated for 25 min at 4 °C. The protein concentration of the samples was adjusted to equal amounts using Pierce BCA Assay Kit (Thermo Fisher Scientific, Waltham, MA, USA) for subsequent immunoprecipitation. 50–100 μg of protein were used for the pull down of FLAG-tagged Kcnq4 proteins with monoclonal anti-FLAG M2 antibody produced in mouse (mouse monoclonal Anti-FLAG M2 antibody, F3165) and Protein G Sepharose beads (Abcam, UK) at 4 °C overnight. For Western blot analysis, beads were boiled in Laemmli sample buffer.

2.16. Biotinylation of reversibly oxidized thiols

The experiment started like the biothinylation of reduced thiols, described above. After H_2O_2 treatment, biotin labeling of reversibly oxidized thiols was conducted by a modified protocol based on Oliver Löwe et al. [23]. Briefly, free thiols were alkylated with 100 mM N-ethylmaleimide (NEM, Sigma-Aldrich, Burlington, MA, USA) in H-medium for 5 min at room temperature. Subsequently, cells were lysed and collected from the plate in ice-cold BASE-buffer (1% IGEPAL-CA630, 150 mM NaCl, 50 mM TRIS, 1 mM EDTA, pH 8) supplemented with 100 mM NEM and cOmplete Mini Protease Inhibitor Cocktail (Merck, Darmstadt, Germany) on ice. Samples were centrifuged at 15,000 RPM for 10 min at 4 °C. Excess of NEM was removed from the supernatants using 0.5 ml Zeba Spin Desalting Columns (Thermo Fisher Scientific, Waltham, MA, USA) according to the manufacturer's recommendations. Reversibly oxidized thiols were reduced with 2.3 mM dithiothreitol (DTT, Avantor, Radnor, PA, USA) for 30 min on ice. Upon removal of excess DTT with desalting columns, reduced thiols were alkylated with biotin polyethyleneoxide iodoacetamide (Thermo Fisher Scientific, Waltham, MA, USA) for 2 h on ice in ultrasound bath. After removal of unbound BIAM with desalting columns, the steps of the biothinylation of reduced thiols as described above were followed. Kcnq4 was immunoprecipitated and signals were detected by Western blot.

2.17. Biotinyl tyramide assay

HaCaT and HaCaT DUOX1 knockout confluent cells on coverslips were washed with H-medium and treated with 1 μM thapsigargin in the

presence or absence of 0.2 U/ml horse radish peroxidase and 27,5 μM biotinyl tyramide (Sigma Aldrich, Burlington, MA, USA) for 5 min at 37 °C. After treatment, cells were washed 3 times with PBS on ice and bound biotinyl tyramide was visualized with fluorescent streptavidin (Vector Laboratories, Inc., Burlingame, CA, USA) at 1:1000 in PBS for 30 min at 4 °C. Cells were fixed with ice-cold 4% paraformaldehyde solution and cell nuclei were stained with To-Pro-3 (Invitrogen). Samples were mounted with Mowiol (Sigma Aldrich, Burlington, MA, USA) and analyzed with an LSM710 confocal laser-scanning microscope using a 63x oil objective (Carl Zeiss).

2.18. Non-commercial DUOX1 antibodies

411-amino-acids-long sequence of recombinant human DUOX1 (amino acids 622–1032) was produced and purified from BL21 Cells and injected intracutaneously with Freund's adjuvant into New Zealand white rabbit.. For polyclonal antibodies rabbits were sacrificed, and antibodies were affinity purified from the sera using Affigel 10 beads (BioRad Laboratories, Hercules, CA, USA) loaded with the antigens according to the manufacturer's instructions.

2.19. DUOX1 CRISPR in HaCaT

HaCaT cells were genetically mutated for DUOX1, using a pSpCas9 (BB)−2A-GFP (PX458, Addgene) vector, following Target Sequence Cloning Protocol by ZhangLab. The vector contained the 5′-gagctgtctcggctgcggacagg-3′ guide sequence. The cells were transfected with Lipofectamine LTX and Plus Reagent (Invitrogen) and GFP-positive cells were sorted onto 96 well plates. Cell clones were screened by PCR of genomic DNA using 5′-gtgcagtgaggatatcccaaccc-3′ sense and 5′-ctggctcctgaccaatgctgg-3′ antisense oligos. PCR products were analyzed by Surveyor mismatch analysis, then sent for sequencing. It was confirmed by Western blot analysis and Amplex Red assay that the selected cell line does not express DUOX1.

2.20. Western blot experiments

Laemmli sample buffer was added to the cell lysate samples and these were run on 8% or 10% SDS polyacrylamide gels and blotted onto nitrocellulose membranes. Membranes were blocked in phosphate buffered saline containing 0,1% Tween- 20 and 5% dry milk. The first antibodies were diluted in blocking buffer and used either for 1 h at room temperature or overnight at 4 °C. After several washing steps in PBS-Tween-20 membranes were incubated with HRP-linked secondary antibodies (Amersham Pharmaceuticals, Amersham, UK) diluted in blocking buffer. After further PBS-Tween-20 washing steps antibody binding was detected using enhanced chemiluminescence and Fuji Super RX medical X-ray films. Importantly samples were never boiled when processed for western blotting with the DUOX1 antibody.

The redox state of Kcnq4 was also measured by immunoblotting. Detection of proteins was performed using HRP-Conjugated Streptavidin (Thermo Fisher Scientific, Waltham, MA, USA) in phosphate buffered saline containing 0,1% Tween- 20 and 5% bovine serum albumin.

2.21. Statistical analysis

Statistical analyses were performed using Graph Pad Prism 7.0 and Origin Pro 8 software programs. Specific statistical tests are presented in the figure legend for each experiment. P-values below 0.05 were considered statistically significant.

3. Results

3.1. Expression and activity of DUOX1 in keratinocytes

We analyzed the expression of NOX/DUOX NADPH oxidases in the mouse skin and mouse primary keratinocytes as well as in the human immortalized keratinocyte cell line (HaCaT) by quantitative reverse transcription PCR. In the mouse tail and paw skin, and also in primary mouse keratinocytes, we found the highest expression levels for DUOX1 and its auxiliary protein DuoxA1 (Fig. 1A–C). In accordance with the results of our previous work [4] immortalized HaCaT keratinocytes also showed strong DUOX1 expression (Fig. 1D). We also analyzed DUOX1 expression at the protein level. As we could not find any commercially available antibody that proved to be specific in DUOX1-knockout controlled experiments, we developed a rabbit polyclonal antibody against a recombinant protein containing amino acids 622–1032 of the human DUOX1 protein. It was expected that the antibody will recognize both the human and mouse samples as the two species show a 91% amino acid identity and 96% similarity in this region of DUOX1. Accordingly, we detected specific DUOX1 Western blot signals in mouse skin, mouse primary keratinocytes, and in HaCaT samples as well (Fig. 1E–G).

To visualize how H_2O_2 is secreted into the intercellular space, we applied a previously described idea [24] to devise a novel fluorescent microscope-based method to detect the DUOX1-dependent production of H_2O_2 on a cultured monolayer of keratinocytes. We added biotinylated tyramide and horseradish peroxidase (HRP) into the medium of thapsigargin-stimulated or non-stimulated wild-type or DUOX1-deficient HaCaT cells. In this reaction, HRP covalently attaches biotinylated tyramide to tyrosine side chains of cell surface proteins. The reaction takes place in the immediate proximity of H_2O_2 production. We then visualized the biotinylated tyramide reagent through incubation with fluorescently labeled streptavidin. Strong tyramide labeling was observed at cell-cell borders of thapsigargin-stimulated wild-type cells (Fig. 1H).

We also assessed H_2O_2 production using the sensitive Amplex Red reagent. To stimulate DUOX1 activity we used reagents that can elicit strong intracellular calcium signals like the endoplasmic reticulum Ca-ATPase inhibitor thapsigargin, the TRPV4 agonist GSK1016790A, and the purinergic receptor agonist ATPγS. We could show that both in mouse primary keratinocytes (Fig. 2A) and in HaCaT cells (Fig. 2B), genetic deletion of DUOX1 completely eliminated the induced H_2O_2 production. Based on an H_2O_2 calibration curve, the rate of H_2O_2 production in HaCaT cells was 2,08 nmol/10^6 cells/hour (± 0,02 nmol), a value similar to that previously found in other epithelial cells [13,25]. These results prove the indispensable role of Duox1 in the ROS production of primary keratinocytes. It is also in agreement with our previous work where we used siRNA knockdown of DUOX1 in HaCaT and A431 cell lines [4].

3.2. Histological analysis of DUOX1-deficient mouse skin

To understand if DUOX1 plays a role in physiological sensory functions of the skin we turned to the analysis of DUOX1-deficient animals. As the structural integrity of the skin – or the lack of it – can fundamentally affect sensory signaling processes, we wanted to establish if there is any discernible change in the structure and differentiation of the mouse skin. This analysis was especially vindicated considering the severe cuticle abnormalities described previously in Duox knock-down *C. elegans* [26,27]. The macroscopic appearance of DUOX1 knockout animals is indistinguishable from wild-type mice. Therefore, we carried out a detailed histological analysis of skin samples of wild-type and DUOX1 knockout mice. Paraffin-embedded tissue sections from mouse tail and paw skin were H&E stained or labeled with specific antibodies (Fig. 3A and B). We used a keratin-14 antibody to mark the proliferative basal layer of the stratified epidermis, keratin-10 and loricrin antibodies for early and late differentiation of keratinocytes (Fig. 3B) connexin-43 and γ-catenin antibodies to show the intercellular connection between keratinocytes through the gap- and tight junctions respectively (Fig. S1). To reveal if there is any possible change in the epidermal organization at the ultrastructural level we studied the stratified epithelium of the

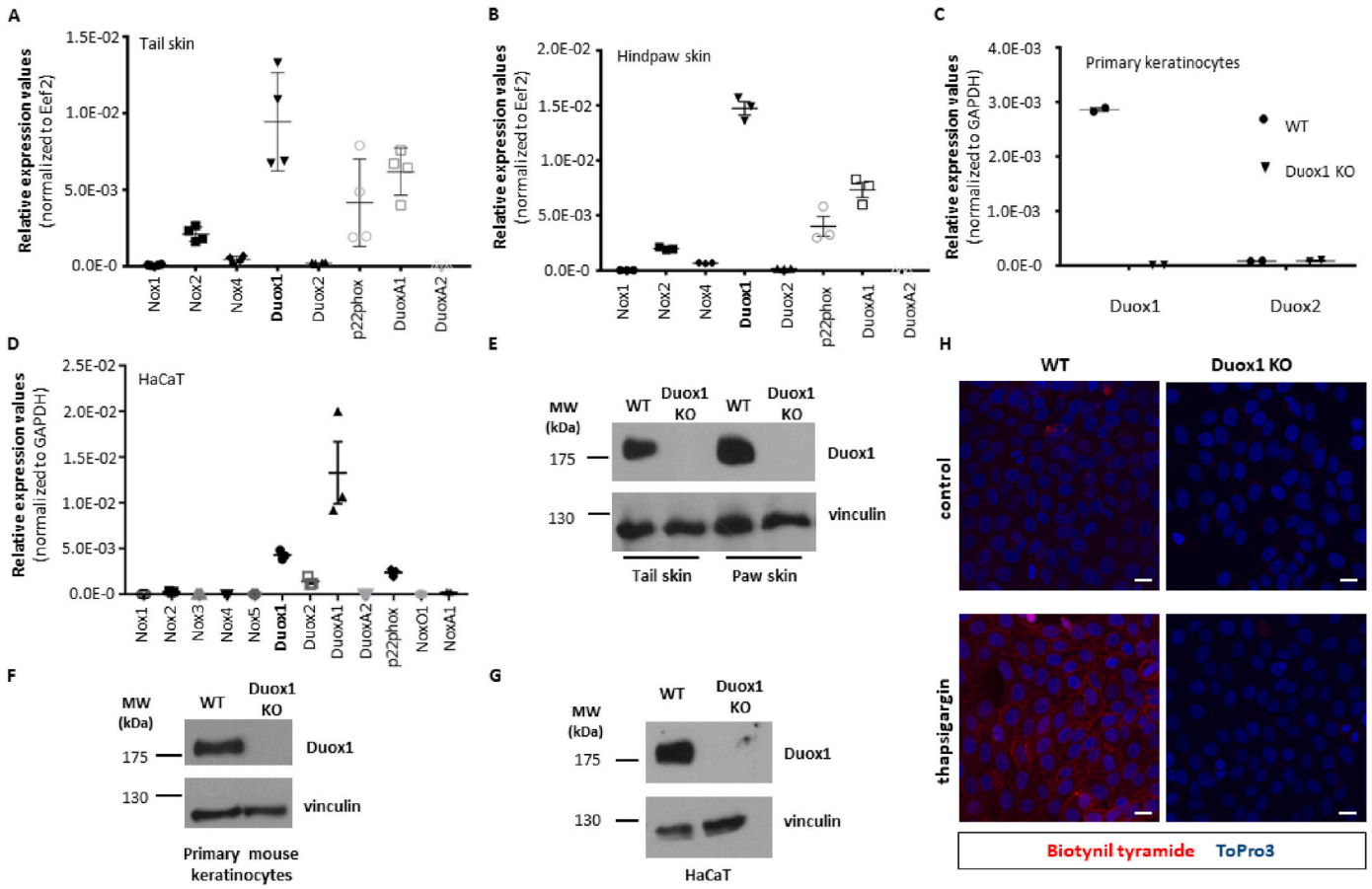

Fig. 1. Expression and activity of Duox1 in epithelial cells. Quantitative PCR analysis of the expression of NADPH oxidase family components in mouse tail skin (*A*), hindpaw skin (*B*), primary mouse keratinocytes (*C*) and HaCaT cells (*D*). Dot plots represent mean ± SEM from 3 to 4 independent experiments. Western blot analysis of Duox1 protein expression in tail skin and hindpaw skin tissue or primary kertinocytes from wild-type and Duox1 knockout mice (*E* and *F*) or HaCaT wild type cells or CRISPR-modified Duox1 knockout cells (*G*). Biotinyl tyramide assay in HaCaT wild-type cells or CRISPR-modified Duox1 knockout cells (*H*). Cells were treated with 1 μM thapsigargin in the presence or absence of horse radish peroxidase. Reaction solution also contained 27.5 μM biotinyl tyramide. After treatment, biotinylated molecules were labeled with fluorescent streptavidin and fixed. Cell nuclei were stained with To-Pro-3. Scale bars: 10 μm.

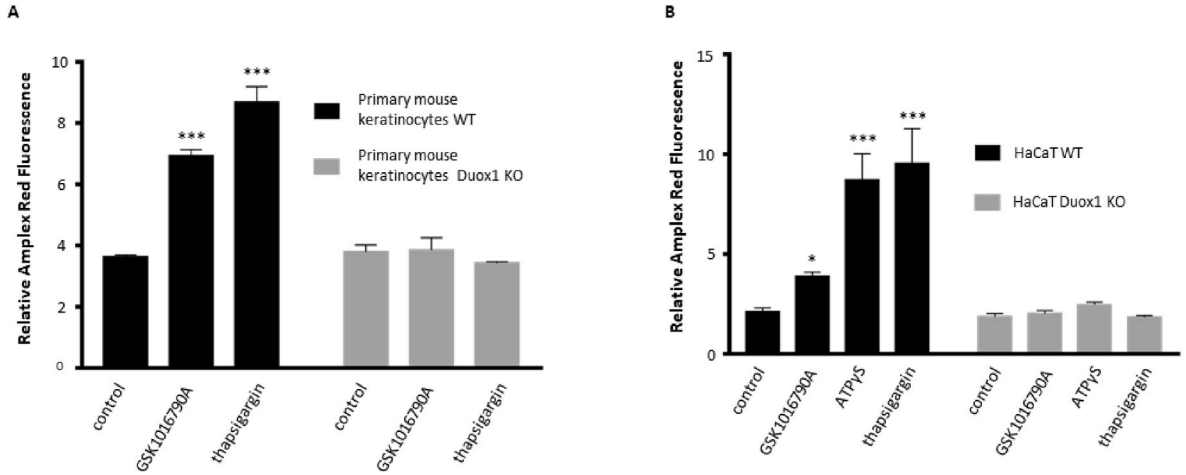

Fig. 2. Measurement of changes in Amplex Red fluorescence. (*A*) Primary mouse back skin keratinocytes were stimulated with 2 nM GSK 1016790A or 100 nM thapsigargin for 30 min. (B) HaCaT wild-type or CRISPR-modified Duox1 knockout cells were stimulated with 2 nM GSK 1016790A or 10 μM ATPγS or 1 μM thapsigargin for 30 min. Cumulative change in Amplex Red fluorescence after 30 min was normalized to the initial fluorescence signal. Representative plot (2 independent experiments for primary cells and 3 independent experiments for HaCaT cells) shows mean ± SD of triplicate. *$p < 0.05$, ***$p < 0.001$ compared with corresponding controls, by 2-way ANOVA.

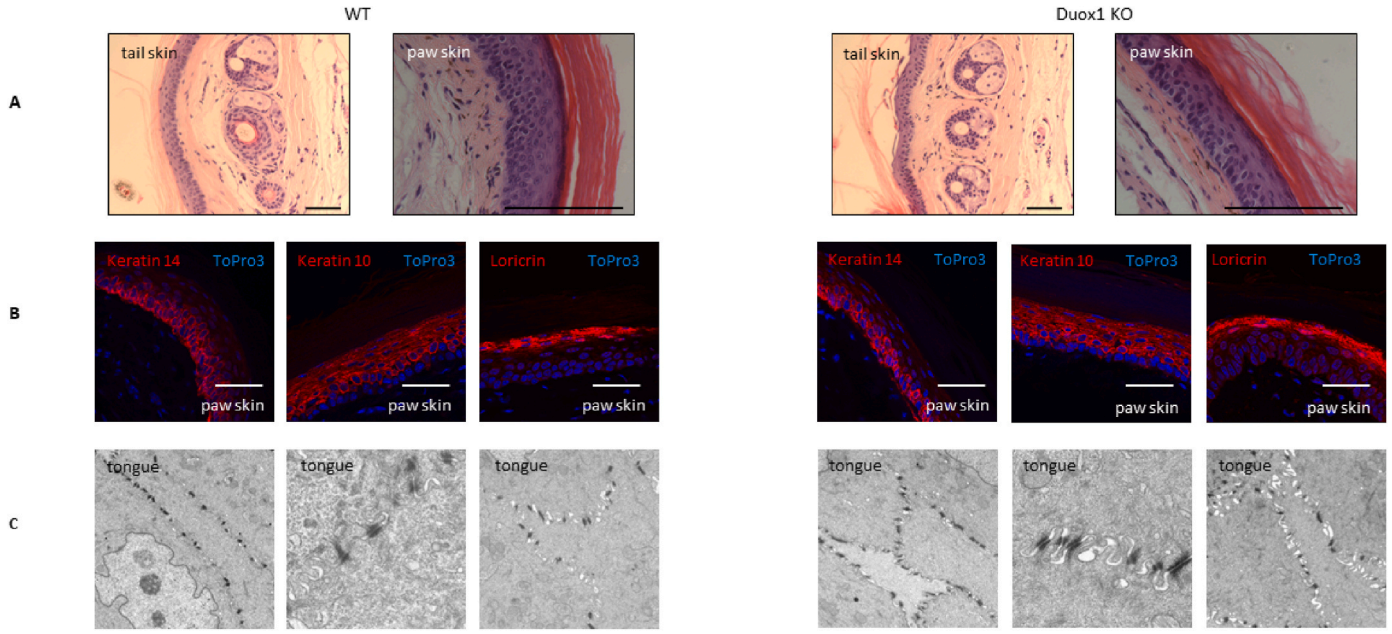

Fig. 3. Histological analysis of wild-type and DUOX1-deficient mouse skin. (*A*) H&E staining of paraffin embedded tissue sections from wild-type and Duox1 KO mouse tail and paw skin. Scale bars: 50 μm. (*B*) Wild-type or Duox1 KO mouse paw skin sections were labeled with keratin-14, keratin-10 and loricrin antibodies. Scale bars: 25 μm. (*C*) Analysis of WT and Duox1 KO mouse tongue by transmission electron microscopy.

mouse tongue by transmission electron microscopic analysis (Fig. 3C). Epidermal nerve fibers can be specifically immunolabeled with antibodies against the PGP9.5 (ubiquitin carboxyl-terminal hydrolase L1) antigen. Using 100 μm thick paraffin sections of paw skin epidermis we could visualize the winding intraepidermal nerve fibers. Also, on tail skin wholemount tissue samples, we could immunolabel intracutaneous nerve fibers using anti-Tuj1 antibodies. However, in both immunolabeling techniques, there were no obvious qualitative changes in density or branching of these nerve fibers (Fig. S2). Based on all these results we concluded that there was no discernible alteration of epidermal differentiation and structure in the skin of DUOX1 knockout mice.

4.3. Selectively altered nociceptive behavior of DUOX1 deficient animals

As the above results demonstrated that DUOX1 is the predominant source of ROS in keratinocytes we analyzed how DUOX1 activity might affect nociceptive functions in mice. We applied various noxious stimuli to the mouse skin in order to unveil potential differences in the nociceptive behavior of DUOX1 deficient animals.

Pretreatment with the TRPA1 agonist allyl-isothiocyanate (mustard oil) on the mouse skin causes the activation of the capsaicin-sensitive sensory nerve terminals, and release of proinflammatory neuropeptides, inducing acute neurogenic inflammation, and consequently increased sensitivity towards thermal stimuli [14]. The decrease of the thermonociceptive threshold (hyperalgesia) is a measurable parameter. As shown in Fig. 4, mustard oil pretreatment (5% for 30 s) of the tail elicited tail removal from the increasing temperature water bath at significantly lower temperatures in DUOX1 knockout animals than in wild-type animals, i.e. the DUOX1 deficient animals were much more sensitized to thermal stimuli than control animals. The difference was visible throughout the entire observation period (10–60 min after the stimuli). This indicated an alleviating effect of DUOX1 activity in the nocifensive behavior elicited by cutaneous thermal stimuli. Importantly, intraperitoneal naloxone pretreatment did not lower the thermal nociceptive threshold in the mice, indicating that endogenous opioid mechanisms do not play a role in this process (Fig. S3).

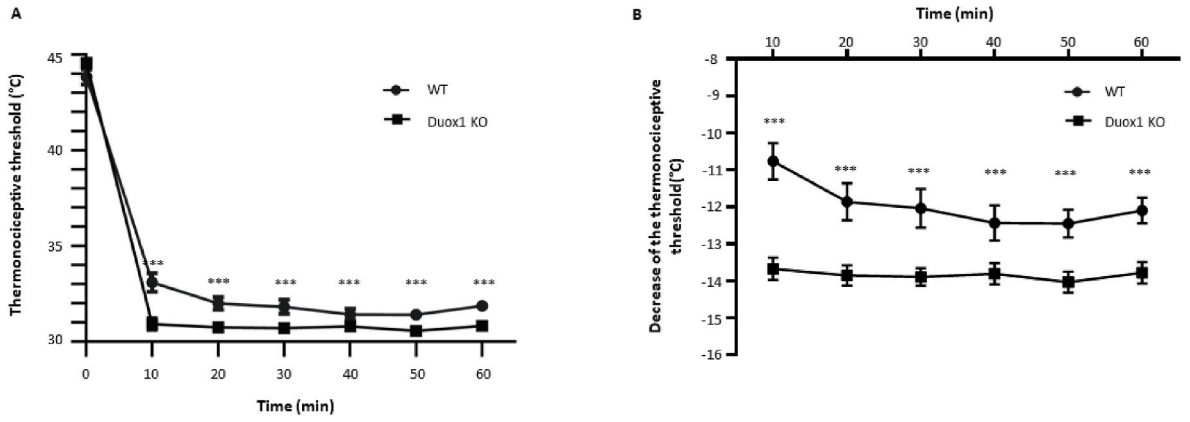

Fig. 4. Allyl isothiocyanate-induced thermal hyperalgesia on the tail of wild-type and Duox1 knockout mouse. (*A* and *B*) Thermal hyperalgesia was induced by allyl isothiocyanate (AITC)-contained mustard oil for 30 s. Comparison of the tail thermonociceptive threshold and its decrease after AITC treatment in wild-type and Duox1 knockout mice. Noxious heat threshold measurements were repeated at 10 min intervals for 60 min after treatment. Plots show mean ± SEM of n = 16–17 animals/group. ***$p < 0.001$ compared with corresponding controls, by 2-way ANOVA.

We also studied the formalin-induced behavioral response following intraplantar formalin injection. Of note, the nocifensive behavior elicited by formalin treatment also involves TRPA1 activation [28]. Although we could not observe a significant difference in paw swelling between wild-type and DUOX1 knockout animals (Fig. S4), we found an increase in both paw lickings and paw flinches in the second phase of observation (Fig. 5A and B) which resulted in a significantly increased composite pain score in DUOX1 deficient animals (Fig. 5C).

In the next experiment, neither noxious heat, nor mechanical nociceptive thresholds following subjection of the animals to a short heat injury (immersing the hind paw into a 51 °C water bath for 15 s under ether anaesthesia) showed significant differences between wild-type and DUOX1 deficient animals (Fig. S5).

Finally, following mechanical noxious stimuli (plantar incision) we measured mechanical nociceptive thresholds in both wild-type and DUOX1 knockout groups, but this postoperative hyperalgesia was not different either in the DUOX1 KO animals compared to wild-type controls (Fig. S6).

In the following experiments, we aimed to identify the possible molecular targets of DUOX1-mediated H_2O_2 production.

3.4. PGE2 and ATP release from stimulated keratinocytes

Keratinocytes can release several mediators that are known to influence nociceptive behavior. We assumed that stimuli that cause an increase in $[Ca^{2+}]_{ic}$ will simultaneously activate DUOX1 and trigger the secretion of mediators as well. Therefore, in stimulated keratinocytes, we can observe if DUOX1 activity can influence the release of mediators. Intraplantar PGE2 is a known inducer of nociceptive behavior [29]and is also described as a secretory product of keratinocytes [30]. We measured the stable adenosine triphosphate analog ATPγS-elicited PGE2-release of scrambled or DUOX1-specific siRNA treated HaCaT cells. As seen in Fig. S7, we could strongly induce the release of PGE2 with ATPγS, however, there was no difference between scrambled and DUOX1 knockdown cells that could explain the previously described behavioral phenotype changes.

ATP is also a frequently studied peripheral nociceptive mediator [31] that can be released from keratinocytes [32]. However, despite our repeated efforts, with the use of commercially available, luminescence-based ATP-release kits we could not measure significant and reproducible ATP signals in the supernatant of keratinocytes. Therefore, we applied a previously described, genetically encoded, GPCR activation-based ATP sensor, $GRAB_{ATP}$ [20]. This sensor construct is based on the insertion of a circularly permutated enhanced GFP (cpEGFP) into the ATP-binding $hP2Y_1$ receptor. The binding of ATP by this fusion construct specifically and sensitively enhances the fluorescence of cpEGFP. We set up a coculture system, where wild-type or DUOX1 deficient HaCaT cells were cocultured with $GRAB_{ATP}$ expressing HEK293A cells. In this system, we selectively stimulated the keratinocytes with the TRPV4 agonist GSK1016790A. This compound does not act on HEK293A cells but induces a strong increase in $[Ca^{2+}]_{ic}$ and DUOX1 activity in keratinocytes [4,33]. Accordingly, GSK1016790A did not elicit any changes in the fluorescence of $GRAB_{ATP}$ expressing HEK293A cells. H_2O_2 treatment did not affect the fluorescence of $GRAB_{ATP}$ either (Fig. S8 and Video S2). Thus we assumed that if GSK1016790A triggers ATP-release then it should specifically activate the $GRAB_{ATP}$ sensors on the membrane of the transfected HEK293A cells. Indeed, we could repeatedly observe transient local oscillations followed by sustained high signals of extracellular ATP in the $GRAB_{ATP}$ expressing HEK293A cells following TRPV4 stimulation of the neighboring keratinocytes (Fig. 6 and Video S1). However, there were no obvious differences between sensor cell activation cocultured with wild-type or DUOX1-deficient HaCaT cells (Fig. 6).

Supplementary data related to this article can be found at https://doi.org/10.1016/j.redox.2023.102670.

3.5. Hydrogen peroxide-mediated redox changes of TRPA1-dependent intracellular calcium signals

Dorsal root ganglion (DRG) neurons express numerous ion channels and membrane receptors that regulate their excitability. Detailed quantitative RNA-sequencing datasets are available about the membrane receptors and ion channels expressed in these neurons [34]. We confirmed the strong expression of several of these ion channels in our own qPCR measurements. Importantly, we could not detect any significant changes in the expression level of these genes between wild-type and DUOX1 KO DRG samples (Fig. 7A). We also analyzed the expression of TRPV3 and TRPV4 in wild-type and DUOX1 knockout mouse skin samples as these heat sensitive receptors have been previously described to play a role in the thermosensory function of the skin [35,36]. However, as shown in Fig. 7B we did not see a DUOX1-dependent change in the expression of these genes. In the following experiments, we aimed to identify molecular targets, the activity of which might be affected by hydrogen peroxide.

We browsed the available literature data to find cell surface proteins of DRG cells that had been reported to show redox-sensitive activity. The H_2O_2 -sensitive TRPA1 channel is present in certain populations of DRG cells [37].

Therefore, first we expressed recombinant TRPA1 channels in HEK293T cells, and followed intracellular calcium signals upon treatment with H_2O_2 and a TRPA1 agonist. As seen in Fig. 8A and Fig. S9A, the TRPA1-expressing HEK cells - in contrast to the non-transfected cells - showed a continuous, H_2O_2-dependent increase in $[Ca^{2+}]_{ic}$. Importantly, following preincubation with H_2O_2, the TRPA1-expressing cells responded to the TRPA1 agonist allyl isothiocyanate (AITC) with a much smaller relative increase in $[Ca^{2+}]_{ic}$ than those cells without an H_2O_2 pretreatment (Fig. 8B and Fig. S9B). This is a clear indication that H_2O_2 has a significant impact on the responsiveness of TRPA1-expressing cells to specific stimuli. These data confirm the idea of keratinocyte-derived H_2O_2 acting as a paracrine mediator on TRPA1 expressing sensory

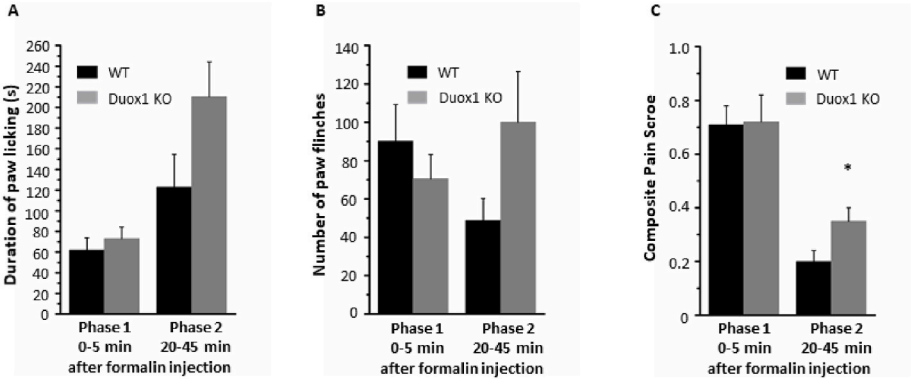

Fig. 5. Formalin-induced nociception in wild-type and Duox1 knockout mouse. After intraplantar 20 μl 2.5% formalin injection, spontaneous nocifensive behaviour was observed between 0-5 min and 20–45 min in wild type and Duox1 KO animals. (*A*) The duration of paw licking was measured by a stopwatch. (*B*) Paw flinching responses were counted. (*C*) Composite Pain Score (CPS) was also calculated by the following formula: CPS=(2x paw licking time + 1x paw flinchings)/observation time. Data are mean ± SEM of n = 5–5 animals/group. *p < 0.05.

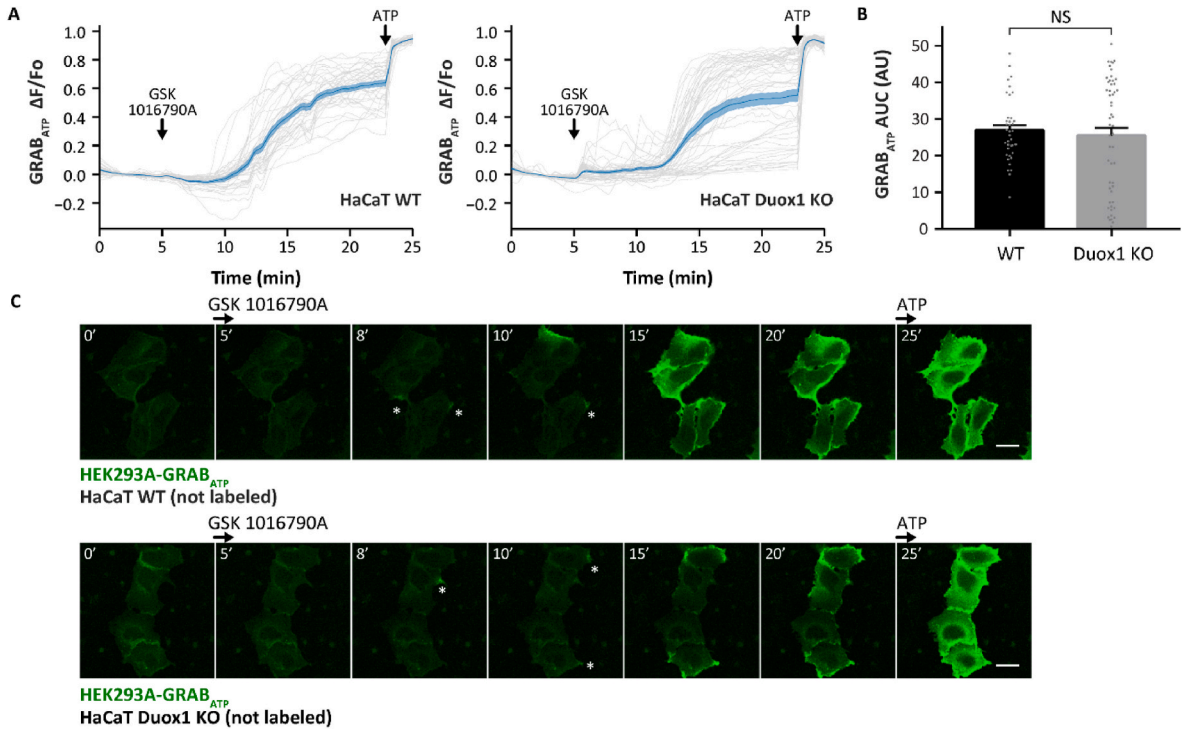

Fig. 6. TRPV4 agonist, GSK 1016790A induced ATP secretion from wild-type and Duox1 knock-out HaCaT cells. (A) Extracellular ATP-sensitive, fluorescent GRABATP sensor expressing HEK293A cells were cocultured with WT or Duox1 knock-out HaCaT. After a wash to remove any residual ATP in the media, the cells were treated with 2.5 nM GSK 1016790A and then with 1 μM ATP, as a positive control. Gray lines represent the normalized mean GRABATP intensity of every cell over time. Blue line shows the overall average of the normalized mean intensity of all the cells ± SEM (WT: n = 38, KO: n = 53 cells from 3 independent experiments). (B) The area under the curve (AUC) was measured for each cell during the time of the GSK 1016790A stimulus, between 5 and 27 min and was plotted per condition (mean ± SEM, gray dots represent values of individual cells). (C) Fluorescent images from different time points showing local oscillations (marked by asterisks) and sustained elevations of the GRABATP signal. Scale bars: 25 μm. (For interpretation of the references to colour in this figure legend, the reader is referred to the Web version of this article.)

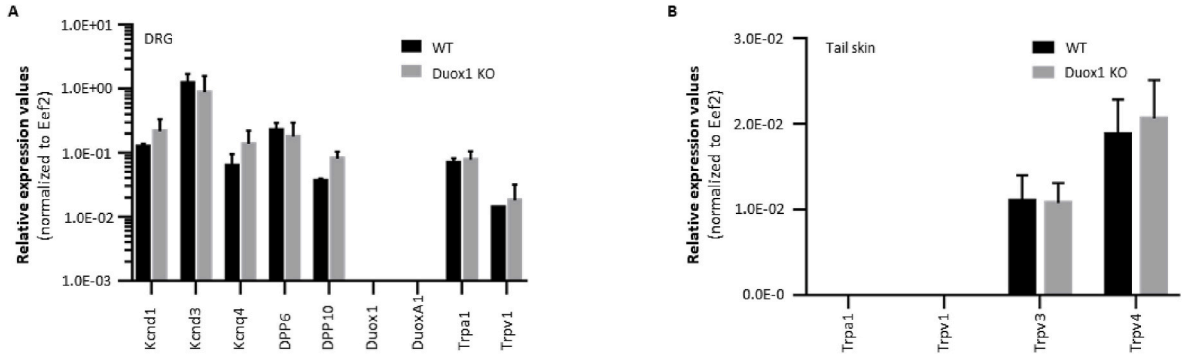

Fig. 7. Expression of ion channels and Duox1 in dorsal root ganglion and tail skin. (*A*) Quantitative PCR analysis of the expression of potassium channels, Duox1, DuoxA1 and TRP channels in wild-type and Duox1 knockout mouse dorsal root ganglion. Bars represent mean ± SEM from 2 independent experiments. (*B*) Quantitative PCR analysis of the expression of TRP channels in mouse tail skin. Bars represent mean ± SEM from 2 to 4 independent experiments.

nerve fibers.

3.6. Expression and H_2O_2 mediated redox changes of Kcnq4 M-type potassium channel

Our next candidate of redox-sensitive ion channels was the voltage-gated M-type potassium channel – Kv7.4 or Kcnq4 – as it was reported in a detailed electrophysiological study to remain in its open state longer after H_2O_2-mediated oxidation [38]. Our qPCR analysis showed that this channel is expressed – in sharp contrast to DUOX1 – very strongly in primary sensory neurons but was hardly detectable in paw and tail skin samples (Fig. 9A and B). We aimed to provide biochemical evidence about the H_2O_2-mediated oxidation of cysteine-thiols in this channel protein. We used biotinylated iodoacetamide (BIAM) to follow the oxidation of the FLAG-tagged, recombinant Kcnq4 potassium channel [39]. In the first set of experiments, we treated Kcnq4-FLAG transfected HEK293 cells with increasing concentrations of hydrogen peroxide and lysed them in the presence of BIAM. Then we carried out an immunoprecipitation with monoclonal anti-FLAG antibody and ran the immunoprecipitate on SDS polyacrylamide gel to test the amount of biotin labeling with streptavidin-HRP. As it is shown in Fig. 9C, the biotin signal decreased as the added H_2O_2 concentration increased indicating the oxidation of sulfhydryl groups of Kcnq4. To confirm these results, and investigate the reversibility of oxidation, we carried out BIAM

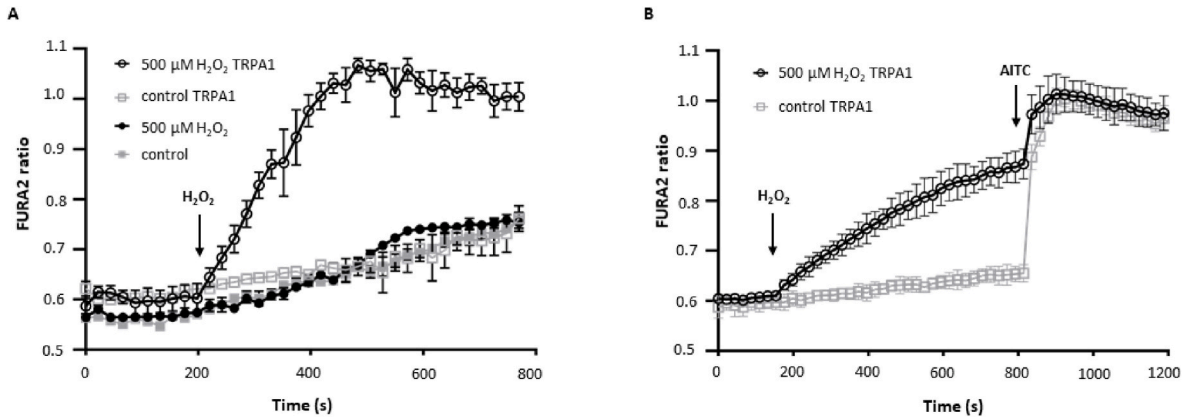

Fig. 8. Ca^{2+} measurements with Fura-2-AM in HEK293 cells expressing TRPA1. (*A*) TRPA1-dependent effect of H_2O_2 on $[Ca^{2+}]_{ic}$. $[Ca^{2+}]_{Ic}$ responses evoked by 500 μM H_2O_2 in the presence of TRPA1. (*B*) Change in $[Ca^{2+}]_{ic}$ of TRPA1 transfected HEK cells in response to sequential applications of 500 μM H_2O_2 and 10 μM AITC. Representative plot from at least 3 independent experiments shows the mean ± SD of triplicate.

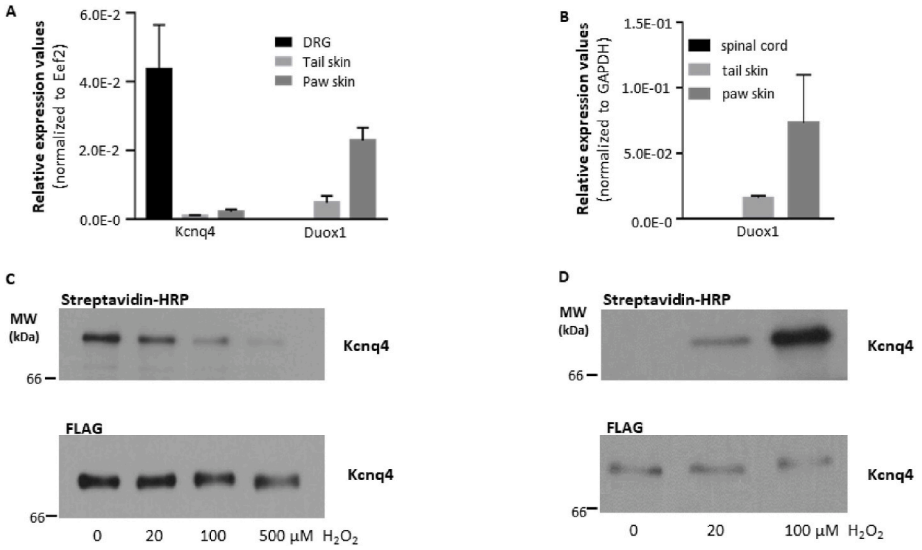

Fig. 9. Hydrogen peroxide mediated redox changes of voltage-gated potassium channel, Kcnq4. (*A*) Quantitative PCR analysis of the Kcnq4 and Duox1 in wild-type mouse dorsal root ganglion, tail skin and paw skin. Bars represent mean ± SEM from 3 independent experiments. (*B*) Expression of Duox1 in spinal cord, tail and paw skin. (*C*) HEK293 cells expressing FLAG-tagged Kcnq4 were treated with H_2O_2 (0, 20, 100, 500 μM) and lysed in presence of BIAM. Following anti-FLAG immunoprecipitation, BIAM signal was detected by streptavidin-HRP on Western blot. (*D*) After H_2O_2 treatment (0, 20, 100 μM) non-oxidized thiols were alkylated with N-ethylmaleimide, then lysates were reduced with dithiothreitol and labeled with BIAM. We continued with anti-FLAG immunoprecipitation and streptavidin-HRP detection.

labeling also in a reverse fashion [23]. In this case, we first alkylated all the non-oxidized sulfhydryl groups after the peroxide treatment using N-ethyl-maleimide (NEM). Subsequently, we reduced all the reversibly oxidized sulfhydryl groups (aka sulphenic acid) with dithiothreitol and carried out the BIAM labeling of reduced cell lysate samples. Then we continued with anti-FLAG immunoprecipitation and streptavidin-HRP detection as described above. This way the streptavidin-HRP signal increased proportionally with the increased oxidation of the potassium channel (Fig. 9D).

In the later version of redox labeling, we observed that high peroxide concentrations (500 μM) eliminated the streptavidin signal indicating an irreversible oxidation – formation of sulfinic or sulfonic acid – of the thiol groups of Kcnq4 which were impossible to reduce with dithiothreitol. These experiments proved that Kcnq4 is present in DRG but not in keratinocytes and is indeed a direct molecular target of H_2O_2-mediated redox changes.

4. Discussion

To our knowledge, the present work is the first to demonstrate the physiological sensory function of NADPH oxidase-derived ROS in the mammalian skin. We analyzed the expression and activity of the members of the NOX/DUOX family of NADPH oxidases in the mouse skin and primary keratinocytes as well as in human immortalized keratinocytes and showed that the predominant member of this family in both mouse and human keratinocytes was DUOX1. We generated a specific, polyclonal antibody against DUOX1 so that we could also confirm its expression at the protein level. We also devised a technique to visualize its hydrogen peroxide-producing activity in epithelial monolayers.

DUOX1 is a transmembrane NADPH oxidase enzyme possessing intracellular Ca^{2+}-binding EF-hands and its activity can be induced through intracellular Ca^{2+} signals. It also carries an extracellular peroxidase homology domain which is inactive in mammalian species. Despite a large number of publications and the recently published detailed structural information about DUOX1 [40], relatively little is known about the physiological functions and biochemical mechanisms of this enzyme. Previously it has been described in various functions, like the airway epithelial wound repair and epithelial responses to allergic and microbial triggers [41–44], the pressure responses of the urinary bladder [13], the activity of primary B-cells [45] or the growth factor elicited redox signaling of epithelial cells [4]. Interestingly, epigenetic downregulation of DUOX1 was reported in different epithelial cancers [46–48]. It has also been shown that DUOX (Ce-DUOX1/-BLI-3) plays an important role in the development and maintenance of the *C. elegans* cuticle [26,27]. Importantly, however, we have not found any structural or ultrastructural differences in the skin of Duox1

deficient mice.

As DUOX1 activity can be triggered by various stimuli in keratinocytes it seemed to be a plausible hypothesis that environmental inputs can affect the sensory function of the skin by altering the DUOX1 oxidase activity. This possibility seemed particularly interesting because keratinocytes are increasingly being recognized as active participants in sensory functions.

It has been shown previously that some molecules, like the Transient Receptor Potential Vanilloid 3 (TRPV3) can play a role in both sensory and barrier functions of the skin [49–51]. As the proper development of the barrier function of the skin can also severely affect its sensitivity towards environmental challenges, it was requisite to thoroughly investigate possible morphological changes in DUOX1 knockout skin. Our detailed histological analysis indicates that there are no structural or developmental defects in DUOX1-deficient mammalian skin.

We found an enhanced response of DUOX1-knockout animals towards thermal nociceptive treatments following allyl-isothiocyanate pretreatment. DUOX1-knockout animals also showed increased nocifensive responses after intraplantar formalin injection. In this regard, it is also a key result of our gene expression analysis that DUOX1 is not expressed in sensory neuronal cells. Importantly we found no difference in mechanonociceptive thresholds. The selective difference in the nocifensive behavior towards thermal stimuli also indicated an altered sensitivity of peripheral nerve endings of the skin. In agreement with these findings, mechanical hyperalgesia is reported to be under different central control than thermal hyperalgesia [52]. As DUOX1 is expressed specifically in epidermal keratinocytes but not in neuronal cells our finding provides a possible therapeutic target to manage peripheral pain conditions without a direct impact on central nervous functions.

We propose that DUOX1 acts as a quickly and reversibly inducible signaling center, the H_2O_2 production of which can influence direct molecular targets in paracrine and/or autocrine fashion. The autocrine way of H_2O_2 action could be the regulation of the release of signaling molecules from keratinocytes. There is a large number of mediators that had been reported to be released from keratinocytes. Adenosine triphosphate, prostaglandins, leukotrienes, TNF-alpha, interleukins, and endogenous opioids have all been reported to be released from keratinocytes [1–3,53]. Out of these, we tested PGE_2 and ATP release, both well known for eliciting nociceptive responses, but we found no differences in DUOX1-deficient keratinocytes. Obviously, we cannot exclude the possibility that the secretion of some other mediators might be affected by DUOX1 activity.

In comparison with the above-described signaling molecules, H_2O_2 has got several favorable properties. It can be produced very quickly, and its secretion cannot be depleted. It has a very small molecular size which may enablea relatively quick diffusion in the extracellular space. Its diffusion through biological membranes may also depend on the presence of aquaporin channel proteins [54]. Finally, there are several enzymatic and non-enzymatic ways to quickly inactivate or metabolize it which contributes to tight regulation of its biological activity [55]. To delineate DUOX1-derived ROS as a paracrine mediator of nociceptive signaling we aimed at identifying possible molecular targets of hydrogen peroxide. We browsed literature data of cell surface proteins expressed on sensory nerve fibers that were reported to display redox sensitivity. We selected TRPA1 and KCNQ4 for further analysis.

In accordance with previous data, H_2O_2 could elicit calcium signals in TRPA1-expressing cells. We found that pretreatment of TRPA1 expressing cells with H_2O_2 resulted in decreased responsiveness to TRPA1 agonists. This suggests a desensitizing action of H_2O_2 on sensory nerves, damping the general reactivity to nociceptive stimuli. Another way to frame this effect of H_2O_2 is that it actually decreases the contrast between the non-stimulated and AITC-stimulated conditions and thereby lowers the S/S_0 ratio in the Weber-Fechner equation. This leads to the increase of the just noticeable difference, the smallest change in stimuli that can be perceived.

We also show biochemical evidence of H_2O_2-mediated KCNQ4 oxidation with as low as 20 μM H_2O_2. Currently, we do not know if KCNQ4 and TRPA1 are present on the same or rather on some different DRG cell populations. The development of specific antibodies suitable for immunohistochemistry will improve our understanding in this regard. However, the slower closure of KCNQ4 channels following exposure to H_2O_2 might also contribute to a slower or reduced peripheral activation of sensory nerve fibers.

It is also very interesting to note that our previous study has demonstrated that DUOX1 plays a regulatory role in the mechanosensing function of urothelial epithelia. The lack of DUOX1 activity in knockout animals resulted in an enhanced frequency of voiding contractions of the bladder [13]. Although this is a different physiological setting compared to cutaneous nociception, it is intriguing that also in this mechanosensory function DUOX1 had a dampening, alleviating effect.

In summary, our results shed light on a hitherto unrecognized physiological sensory function of DUOX1 in the skin. We pinpointed potential molecular targets of the DUOX1-derived hydrogen peroxide. We believe that H_2O_2-mediated effects include - but are probably not limited to - these molecules. Our data suggest a subtle, physiological regulatory role for ROS in sensory functions. This is rather in contrast to the previous conception of ROS as a pain enhancer factor [56,57]. The main difference in the interpretation of the role of ROS lies probably in the source and regulation of ROS release. Robust ROS production by tissue invading leukocytes in the setting of a tissue injury or severe inflammation is very different from the continuous, small-scale, physiological ROS production of keratinocytes in the intact epidermis.

Our results about ROS released from keratinocytes might open a new path to a more detailed understanding of nociceptive and analgesic signaling pathways in the skin. Further analysis of molecules affected by keratinocyte-derived H_2O_2 can provide actionable molecular targets.

This can contribute to local treatments of pain states without the side effects of systemic therapy.

Funding

This study was supported by grants from the National Research, Development and Innovation Office (PD138404, K133002, NVKP_16-1-2016-0039). The work was also financed by the Thematic Excellence Program 2021 Health Subprogram (MOLORKIV) of the Ministry for Innovation and Technology in Hungary under project no. TKP2021-EGA-24 from the National Research, Development and Innovation Fund and by grants VEKOP-2.3.2-16-2016-00002 and EFOP-3.6.3-VEKOP-16-2017-00009. This project was also supported by the National Research, Development and Innovation Office (PharmaLab, RRF-2.3.1-21-2022-00015), Eötvos Loránd Research Network, TKP2021-EGA-16 has been implemented with the support provided from the National Research, Development and Innovation Fund of Hungary, and OTKA K-138046.

A.P. was supported by a predoctoral grant EFOP-3.6.3-VEKOP-16-2017-00009. B.E. was supported by a “Lendület” grant from the Hungarian Academy of Sciences (LP2018-13/2018) and funding from EU’s Horizon 2020 research and innovation program (grant agreement No. 739593).

Declaration of competing interest

The authors declare that they have no conflict of interest.

Data availability

Data will be made available on request.

Acknowledgements

We are grateful to Beáta Molnár, Barbara Bodor-Kis, Dóra Ömböli and Dóra Rónaszéki for technical assistance. We also appreciate the

expert help of Zoltán Nusser in electron microscopy. We are thankful for the work of the animal facility technicians Klára Papp and Ádám Marinkás.

Appendix A. Supplementary data

Supplementary data to this article can be found online at https://doi.org/10.1016/j.redox.2023.102670.

References

[1] H.E. Burrell, B. Wlodarski, B.J. Foster, K.A. Buckley, G.R. Sharpe, J.M. Quayle, A. W.M. Simpson, J.A. Gallagher, Human keratinocytes release ATP and utilize three mechanisms for nucleotide interconversion at the cell surface, J. Biol. Chem. (2005) 280, https://doi.org/10.1074/jbc.M505381200.

[2] J. Ansel, P. Perry, J. Brown, D. Damm, T. Phan, C. Hart, T. Luger, S. Hefeneider, Cytokine modulation of keratinocyte cytokines, J. Invest. Dermatol. 94 (1990), https://doi.org/10.1111/1523-1747.ep12876053.

[3] T. Andoh, N. Katsube, M. Maruyama, Y. Kuraishi, Involvement of leukotriene b4 in substance p-induced itch- associated response in mice, J. Invest. Dermatol. 117 (2001), https://doi.org/10.1046/j.0022-202x.2001.01585.x.

[4] G. Sirokmány, A. Pató, M. Zana, Á. Donkó, A. Bíró, P. Nagy, M. Geiszt, Epidermal growth factor-induced hydrogen peroxide production is mediated by dual oxidase 1, Free Radic. Biol. Med. 97 (2016) 204–211, https://doi.org/10.1016/j.freeradbiomed.2016.05.028.

[5] M. Talagas, N. Lebonvallet, R. Leschiera, G. Sinquin, P. Elies, M. Haftek, J. P. Pennec, D. Ressnikoff, V. la Padula, R. le Garrec, K. L'herondelle, O. Mignen, L. le Pottier, N. Kerfant, A. Reux, P. Marcorelles, L. Misery, Keratinocytes communicate with sensory neurons via synaptic-like contacts, Ann. Neurol. 88 (2020), https://doi.org/10.1002/ana.25912.

[6] M. Hilliges, L. Wang, O. Johansson, Ultrastructural evidence for nerve fibers within all vital layers of the human epidermis, J. Invest. Dermatol. 104 (1995), https://doi.org/10.1111/1523-1747.ep12613631.

[7] M.G. Porubcin, P. Novak, Diagnostic accuracy of electrochemical skin conductance in the detection of sudomotor fiber loss, Front. Neurol. 11 (2020), https://doi.org/10.3389/fneur.2020.00273.

[8] P. Nagy, A.J. Kettle, C.C. Winterbourn, Neutrophil-mediated oxidation of enkephalins via myeloperoxidase-dependent addition of superoxide, Free Radic. Biol. Med. 49 (2010), https://doi.org/10.1016/j.freeradbiomed.2010.05.033.

[9] Z. Khalil, T. Liu, R.D. Helme, Free radicals contribute to the reduction in peripheral vascular responses and the maintenance of thermal hyperalgesia in rats with chronic constriction injury, Pain 79 (1999), https://doi.org/10.1016/S0304-3959(98)00143-2.

[10] M.M. Khattab, TEMPOL, a membrane-permeable radical scavenger, attenuates peroxynitrite- and superoxide anion-enhanced carrageenan-induced paw edema and hyperalgesia: a key role for superoxide anion, Eur. J. Pharmacol. 548 (2006), https://doi.org/10.1016/j.ejphar.2006.08.007.

[11] M.I. Rashid, A. Ali, S. Andleeb, Functional annotation and analysis of dual oxidase 1 (DUOX1): a potential anti-pyocyanin immune component, Interdiscip Sci 11 (2019), https://doi.org/10.1007/s12539-018-0308-1.

[12] M.R. Romero, J.M. Carroll, F.M. Watt, Analysis of cultured keratinocytes from a transgenic mouse model of psoriasis: effects of suprabasal integrin expression on keratinocyte adhesion, proliferation and terminal differentiation, Exp. Dermatol. 8 (1999), https://doi.org/10.1111/j.1600-0625.1999.tb00348.x.

[13] A. Donkó, E. Ruisanchez, A. Orient, B. Enyedi, R. Kapui, Z. Péterfi, X. de Deken, Z. Benyó, M. Geiszt, Urothelial cells produce hydrogen peroxide through the activation of Duox1, Free Radic. Biol. Med. (2010), https://doi.org/10.1016/j.freeradbiomed.2010.09.027.

[14] V. Tékus, Á. Horváth, Z. Hajna, É. Borbély, K. Bölcskei, M. Boros, E. Pintér, Z. Helyes, G. Petho, J. Szolcsányi, Noxious heat threshold temperature and pronociceptive effects of allyl isothiocyanate (mustard oil) in TRPV1 or TRPA1 gene-deleted mice, Life Sci. 154 (2016), https://doi.org/10.1016/j.lfs.2016.04.030.

[15] K. Bölcskei, Z. Helyes, Á. Szabó, K. Sándor, K. Elekes, J. Németh, R. Almási, E. Pintér, G. Petho, J. Szolcsányi, Investigation of the role of TRPV1 receptors in acute and chronic nociceptive processes using gene-deficient mice, Pain (2005) 117, https://doi.org/10.1016/j.pain.2005.06.024.

[16] E.M. Pogatzki, S.N. Raja, A mouse model of incisional pain materials and methods, Anesthesiology 99 (2003).

[17] K.M. Braun, C. Niemann, U.B. Jensen, J.P. Sundberg, V. Silva-Vargas, F.M. Watt, Manipulation of stem cell proliferation and lineage commitment: visualisation of label-retaining cells in wholemounts of mouse epidermis, Development 130 (2003), https://doi.org/10.1242/dev.00703.

[18] A. Lörincz, T. Notomi, G. Tamás, R. Shigemoto, Z. Nusser, Polarized and compartment-dependent distribution of HCN1 in pyramidal cell dendrites, Nat. Neurosci. 5 (2002), https://doi.org/10.1038/nn962.

[19] M. Kollo, N.B. Holderith, Z. Nusser, Novel subcellular distribution pattern of A-Type K+ channels on neuronal surface, J. Neurosci. 26 (2006), https://doi.org/10.1523/JNEUROSCI.5257-05.2006.

[20] Z. Wu, K. He, Y. Chen, H. Li, S. Pan, B. Li, T. Liu, F. Xi, F. Deng, H. Wang, J. Du, M. Jing, Y. Li, A sensitive GRAB sensor for detecting extracellular ATP in vitro and in vivo, Neuron 110 (2022), https://doi.org/10.1016/j.neuron.2021.11.027.

[21] C. Stringer, T. Wang, M. Michaelos, M. Pachitariu, Cellpose: a generalist algorithm for cellular segmentation, Nat. Methods 18 (2021), https://doi.org/10.1038/s41592-020-01018-x.

[22] G. Pozsgai, M. Payrits, É. Sághy, R. Sebestyén-Bátai, E. Steen, É. Szőke, Z. Sándor, M. Solymár, A. Garami, P. Orvos, L. Tálosi, Z. Helyes, E. Pintér, Analgesic effect of dimethyl trisulfide in mice is mediated by TRPA1 and sst4 receptors, Nitric Oxide (2017) 65, https://doi.org/10.1016/j.niox.2017.01.012.

[23] O. Löwe, F. Rezende, J. Heidler, I. Wittig, V. Helfinger, R.P. Brandes, K. Schröder, BIAM switch assay coupled to mass spectrometry identifies novel redox targets of NADPH oxidase 4, Redox Biol. 21 (2019), https://doi.org/10.1016/j.redox.2019.101125.

[24] J.M. Larios, R. Budhiraja, B.L. Fanburg, V.J. Thannickal, Oxidative protein cross-linking reactions involving L-tyrosine in transforming growth factor-β1-stimulated fibroblasts, J. Biol. Chem. (2001) 276, https://doi.org/10.1074/jbc.M100426200.

[25] B. Rada, H.E. Boudreau, J.J. Park, T.L. Leto, Histamine stimulates hydrogen peroxide production by bronchial epithelial cells via histamine H1 receptor and dual oxidase, Am. J. Respir. Cell Mol. Biol. 50 (2014), https://doi.org/10.1165/rcmb.2013-0254OC.

[26] W.A. Edens, L. Sharling, G. Cheng, R. Shapira, J.M. Kinkade, T. Lee, H.A. Edens, X. Tang, C. Sullards, D.B. Flaherty, G.M. Benian, J. David Lambeth, Tyrosine cross-linking of extracellular matrix is catalyzed by Duox, a multidomain oxidase/peroxidase with homology to the phagocyte oxidase subunit gp91phox, JCB (J. Cell Biol.) 154 (2001) 879–891, https://doi.org/10.1083/jcb.200103132.

[27] R.S. Kamath, A.G. Fraser, Y. Dong, G. Poulin, R. Durbin, M. Gotta, A. Kanapink, N. le Bot, S. Moreno, M. Sohrmann, D.P. Welchman, P. Zipperlen, J. Ahringer, Systematic Functional Analysis of the Caenorhabditis elegans Genome Using RNAi, 2003. www.nature.com/nature.

[28] T. Hoffmann, F. Klemm, T. I Kichko, S.K. Sauer, K. Kistner, B. Riedl, P. Raboisson, L. Luo, A. Babes, L. Kocher, G. Carli, M.J.M. Fischer, P.W. Reeh, The formalin test does not probe inflammatory pain but excitotoxicity in rodent skin, Phys. Rep. 10 (2022), https://doi.org/10.14814/phy2.15194.

[29] J.M. Keppel Hesselink, D.J. Kopsky, A.K. Bhaskar, Skin matters! The role of keratinocytes in nociception: a rational argument for the development of topical analgesics, J. Pain Res. 10 (2017), https://doi.org/10.2147/JPR.S122765.

[30] S.M. Huang, H. Lee, M.K. Chung, U. Park, Y.Y. Yin, H.B. Bradshaw, P.A. Coulombe, J.M. Walker, M.J. Caterina, Overexpressed transient receptor potential vanilloid 3 ion channels in skin keratinocytes modulate pain sensitivity via prostaglandin E2, J. Neurosci. 28 (2008), https://doi.org/10.1523/JNEUROSCI.5741-07.2008.

[31] M.J. Caterina, D. Julius, Sense and specificity: a molecular identity for nociceptors, Curr. Opin. Neurobiol. 9 (1999), https://doi.org/10.1016/S0959-4388(99)00009-4.

[32] N. Mizumoto, M.E. Mummert, D. Shalhevet, A. Takashima, Keratinocyte ATP release assay for testing skin-irritating potentials of structurally diverse chemicals, J. Invest. Dermatol. 121 (2003), https://doi.org/10.1046/j.1523-1747.2003.12558.x.

[33] J. Luo, J. Feng, G. Yu, P. Yang, M.R. Mack, J. Du, W. Yu, A. Qian, Y. Zhang, S. Liu, S. Yin, A. Xu, J. Cheng, Q. Liu, R.G. O'neil, Y. Xia, L. Ma, S.M. Carlton, B.S. Kim, K. Renner, Q. Liu, H. Hu, TRPV4-expressing macrophages and keratinocytes contribute differentially to allergic and non-allergic chronic itch HHS public access, J. Allergy Clin. Immunol. 141 (2018) 608–619, https://doi.org/10.1016/j.jaci.2017.05.051.

[34] S. Manteniotis, R. Lehmann, C. Flegel, F. Vogel, A. Hofreuter, B.S.P. Schreiner, J. Altmüller, C. Becker, N. Schöbel, H. Hatt, G. Gisselmann, Comprehensive RNA-Seq expression analysis of sensory ganglia with a focus on ion channels and GPCRs in trigeminal ganglia, PLoS One 8 (2013), https://doi.org/10.1371/journal.pone.0079523.

[35] S.M. Huang, X. Li, Y.Y. Yu, J. Wang, M.J. Caterina, TRPV3 and TRPV4 ion channels are not major contributors to mouse heat sensation, Mol. Pain 7 (2011), https://doi.org/10.1186/1744-8069-7-37.

[36] W.C. Wetsel, Sensing hot and cold with TRP channels, Int. J. Hyperther. 27 (2011), https://doi.org/10.3109/02656736.2011.554337.

[37] D.A. Andersson, C. Gentry, S. Moss, S. Bevan, Transient receptor potential A1 is a sensory receptor for multiple products of oxidative stress, J. Neurosci. 28 (2008), https://doi.org/10.1523/JNEUROSCI.5369-07.2008.

[38] N. Gamper, O. Zaika, Y. Li, P. Martin, C.C. Hernandez, M.R. Perez, A.Y.C. Wang, D. B. Jaffe, M.S. Shapiro, Oxidative modification of M-type K+ channels as a mechanism of cytoprotective neuronal silencing, EMBO J. 25 (2006) 4996–5004, https://doi.org/10.1038/sj.emboj.7601374.

[39] T.F. Brewer, F.J. Garcia, C.S. Onak, K.S. Carroll, C.J. Chang, Chemical approaches to discovery and study of sources and targets of hydrogen peroxide redox signaling through NADPH oxidase proteins, Annu. Rev. Biochem. 84 (2015), https://doi.org/10.1146/annurev-biochem-060614-034018.

[40] J.X. Wu, R. Liu, K. Song, L. Chen, Structures of human dual oxidase 1 complex in low-calcium and high-calcium states, Nat. Commun. 12 (2021), https://doi.org/10.1038/s41467-020-20466-9.

[41] U.v. Wesley, P.F. Bove, M. Hristova, S. McCarthy, A. van der Vliet, Airway epithelial cell migration and wound repair by ATP-mediated activation of dual oxidase 1, J. Biol. Chem. 282 (2007) 3213–3220, https://doi.org/10.1074/jbc.M606533200.

[42] A.W. Boots, M. Hristova, D.I. Kasahara, G.R.M.M. Haenen, A. Bast, A. van der Vliet, ATP-mediated activation of the NADPH oxidase DUOX1 mediates airway epithelial responses to bacterial stimuli, J. Biol. Chem. 284 (2009) 17858–17867, https://doi.org/10.1074/jbc.M809761200.

[43] M. Hristova, A. Habibovic, C. Veith, Y.M.W. Janssen-Heininger, A.E. Dixon, M. Geiszt, A. van der Vliet, Airway epithelial dual oxidase 1 mediates allergen-induced IL-33 secretion and activation of type 2 immune responses, J. Allergy Clin.

Immunol. 137 (2016) 1545–1556.e11, https://doi.org/10.1016/j.jaci.2015.10.003.
[44] D. Sarr, A.D. Gingerich, N.M. Asthiwi, F. Almutairi, G.A. Sautto, J. Ecker, T. Nagy, M.B. Kilgore, J.D. Chandler, T.M. Ross, R.A. Tripp, B. Rada, Dual oxidase 1 promotes antiviral innate immunity, Proc. Natl. Acad. Sci. U. S. A. 118 (2021), https://doi.org/10.1073/pnas.2017130118.
[45] R. Sugamata, A. Donko, Y. Murakami, H.E. Boudreau, C.-F. Qi, J. Kwon, T.L. Leto, Duox1 regulates primary B cell function under the influence of IL-4 through BCR-mediated generation of hydrogen peroxide, J. Immunol. (2019) 202, https://doi.org/10.4049/jimmunol.1601395.
[46] S. Luxen, S.A. Belinsky, U.G. Knaus, Silencing of DUOX NADPH oxidases by promoter hypermethylation in lung cancer, Cancer Res. 68 (2008), https://doi.org/10.1158/0008-5472.CAN-07-5782.
[47] A.C. Little, D. Sham, M. Hristova, K. Danyal, D.E. Heppner, R.A. Bauer, L.M. Sipsey, A. Habibovic, A. van der Vliet, DUOX1 silencing in lung cancer promotes EMT, cancer stem cell characteristics and invasive properties, Oncogenesis 5 (2016), https://doi.org/10.1038/oncsis.2016.61.
[48] Q. Ling, W. Shi, C. Huang, J. Zheng, Q. Cheng, K. Yu, S. Chen, H. Zhang, N. Li, M. Chen, Epigenetic silencing of dual oxidase 1 by promoter hypermethylation in human hepatocellular carcinoma, Am J Cancer Res 4 (2014).
[49] A. Moqrich, S.W. Hwang, T.J. Earley, M.J. Petrus, A.N. Murray, K.S.R. Spencer, M. Andahazy, G.M. Story, A. Patapoutian, Impaired thermosensation in mice lacking TRPV3, a heat and camphor sensor in the skin, Science (1979) 307, https://doi.org/10.1126/science.1108609, 2005.
[50] X. Cheng, J. Jin, L. Hu, D. Shen, X. ping Dong, M.A. Samie, J. Knoff, B. Eisinger, M. L. Liu, S.M. Huang, M.J. Caterina, P. Dempsey, L.E. Michael, A.A. Dlugosz, N. C. Andrews, D.E. Clapham, H. Xu, TRP channel regulates EGFR signaling in hair morphogenesis and skin barrier formation, Cell 141 (2010), https://doi.org/10.1016/j.cell.2010.03.013.
[51] S.M. Huang, X. Li, Y.Y. Yu, J. Wang, M.J. Caterina, TRPV3 and TRPV4 ion channels are not major contributors to mouse heat sensation, Mol. Pain 7 (2011), https://doi.org/10.1186/1744-8069-7-37.
[52] Y. Otsubo, Y. Satoh, M. Kodama, Y. Araki, M. Satomoto, E. Sakamoto, G. Pagès, J. Pouysségur, S. Endo, T. Kazama, Mechanical allodynia but not thermal hyperalgesia is impaired in mice deficient for ERK2 in the central nervous system, Pain (2012) 153, https://doi.org/10.1016/j.pain.2012.07.020.
[53] P.L. Bigliardi, D.J. Tobin, C. Gaveriaux-Ruff, M. Bigliardi-Qi, Opioids and the skin - where do we stand? Exp. Dermatol. 18 (2009) https://doi.org/10.1111/j.1600-0625.2009.00844.x.
[54] G.P. Bienert, A.L.B. Møller, K.A. Kristiansen, A. Schulz, I.M. Møller, J. K. Schjoerring, T.P. Jahn, Specific aquaporins facilitate the diffusion of hydrogen peroxide across membranes, J. Biol. Chem. (2007) 282, https://doi.org/10.1074/jbc.M603761200.
[55] H. Sies, V.v. Belousov, N.S. Chandel, M.J. Davies, D.P. Jones, G.E. Mann, M. P. Murphy, M. Yamamoto, C. Winterbourn, Defining roles of specific reactive oxygen species (ROS) in cell biology and physiology, Nat. Rev. Mol. Cell Biol. 23 (2022), https://doi.org/10.1038/s41580-022-00456-z.
[56] D. Salvemini, J.W. Little, T. Doyle, W.L. Neumann, Roles of reactive oxygen and nitrogen species in pain, Free Radic. Biol. Med. 51 (2011), https://doi.org/10.1016/j.freeradbiomed.2011.01.026.
[57] Z.Q. Wang, F. Porreca, S. Cuzzocrea, K. Galen, R. Lightfoot, E. Masini, C. Muscoli, V. Mollace, M. Ndengele, H. Ischiropoulos, D. Salvemini, A newly identified role for superoxide in inflammatory pain, J. Pharmacol. Exp. Therapeut. 309 (2004), https://doi.org/10.1124/jpet.103.064154.